Multi-Wavelength Investigations of Solar Activity
Proceedings IAU Symposium No. 223, 2004
A.V. Stepanov, E.E. Benevolenskaya & A.G. Kosovichev, eds.

DOI: 10.1017/S1743921304005071

Solar-cycle variations in the spectrum of supergranulation

Laurent Gizon[1] and Thomas L. Duvall, Jr[2]

[1]Hansen Experimental Physics Laboratory, Stanford University, Stanford, CA 94305, USA

[2]Laboratory for Astronomy and Solar Physics, NASA/GSFC, Greenbelt, MA 20771, USA

Abstract. Using local helioseismology, we construct maps of the horizontal divergence of the velocity field near the solar surface and study the spectrum of solar supergranulation during the period from 1996 to 2002. Supergranulation oscillates and propagates like a wave interference pattern. The variations of the oscillation frequency with latitude and time are less than 5%. We find significant solar-cycle variations in the lifetime and the anisotropic distribution of power. We also measure the time-dependent zonal and meridional flows that advect supergranules.

1. Observations

To study supergranulation we use series of full-disk Doppler velocity images obtained during the period 1996–2002 by the Michelson Doppler Imager (two to three months each year). Dopplergrams are tracked at the Carrington rotation rate. We apply the techniques of f-mode time-distance helioseismology (Duvall & Gizon 2000) to obtain every 12 h a $120^\circ \times 120^\circ$ map of the horizontal divergence of the flows in a 1-Mm deep layer below the Sun's surface. The maps are interpolated onto a longitude-latitude grid, (ϕ', λ'), sampled at $\delta = 0.24^\circ$ in both coordinates.

For any given target latitude, λ, we consider a section of the data 10°-wide in latitude with $|\lambda' - \lambda| < 5^\circ$. These data are rearranged in a frame of reference with angular velocity $\Omega_{\rm ref}(\lambda) = 14.43^\circ - 1.77^\circ \sin^2\lambda - 2.58^\circ \sin^4\lambda$ day^{-1} (rotation rate of small magnetic features; Komm *et al.* 1993). This choice of reference is convenient, although arbitrary. We use a local-plane approximation in the neighborhood of latitude λ by defining the position vector $\boldsymbol{x} = (x, y)$ with $x = R(\lambda' - \lambda)\cos\lambda$ and $y = R\phi'$ where R is the solar radius. We choose a spatial sampling of $R\delta = 2.92$ Mm in both coordinates x (prograde) and y (northward). The signal is then decomposed into its harmonic components $\exp(i\boldsymbol{k}\cdot\boldsymbol{x} - i\omega t)$ through FFT, where ω is the angular frequency and $\boldsymbol{k} = (k_x, k_y)$ is the wavevector. We compute the power spectrum of the divergence signal, denoted by $P(\boldsymbol{k}, \omega)$, for each target latitude λ (5° steps) and for each year. By convention the direction of the wavector, the *azimuth* ψ, is such that $\boldsymbol{k} = (k\cos\psi, k\sin\psi)$ where $k = \|\boldsymbol{k}\|$. In particular, $\psi = 0$ when $\boldsymbol{k}$ points prograde and $\psi = 90^\circ$ when $\boldsymbol{k}$ points north.

2. Model power spectra

Assuming that the observed power spectrum of the divergence signal, $P(\boldsymbol{k}, \omega)$, may be approximated by the ω-convolution of the solar power spectrum with the power in the observation window, $W(\omega)$, there exists a function $F(\boldsymbol{k}, \omega)$ such that

$$P(\boldsymbol{k}, \omega) = \frac{1}{2}\left[F(\boldsymbol{k}, \omega) + F(-\boldsymbol{k}, -\omega)\right] \otimes W(\omega)\ . \tag{2.1}$$

In this form, the property $P(-\boldsymbol{k}, -\omega) = P(\boldsymbol{k}, \omega)$ is explicit (the divergence signal is real). Gizon *et al.* (2003) discovered that the data can be represented accurately by the

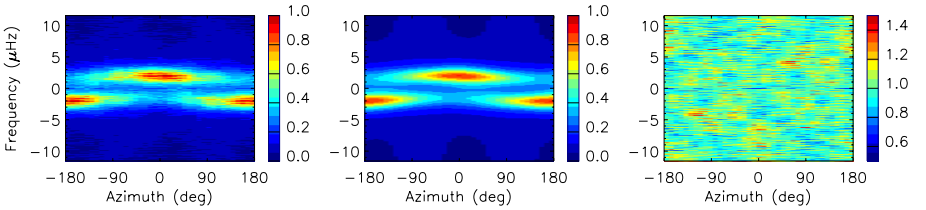

Figure 1. Power spectrum of the divergence signal for $\lambda = 0$ (equator) in 1997. The left panel shows a cylindrical section at constant wavenumber $k = 115/R$, as a function of azimuth, ψ, and frequency, $\omega/2\pi$. The middle panel is a fit to the data according to the model described in the text. In particular, $\eta = 1.15$ and $\psi_{\max} = -2^\circ$ (excess power in the prograde direction). The right panel shows the ratio of the data to the fit.

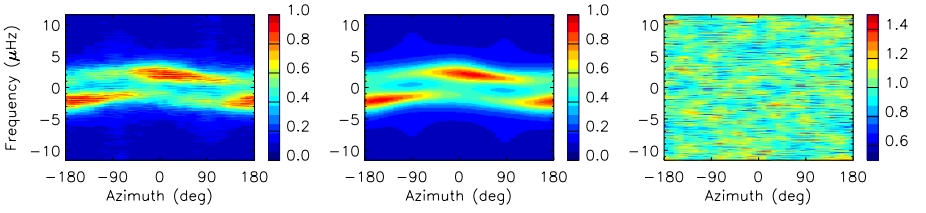

Figure 2. Same as previous figure but for latitude $\lambda = -25^\circ$. The fit returns the values $\eta = 0.82$ and $\psi_{\max} = 29^\circ$, i.e. the power is maximum in a direction that points 29° equatorward of the prograde direction.

parametric model

$$F(\boldsymbol{k},\omega) = \frac{A(\boldsymbol{k})}{1 + [\omega - \omega_{\rm r}(\boldsymbol{k})]^2/\gamma(k)^2} + B(\boldsymbol{k}) \quad \text{with} \quad \omega_{\rm r}(\boldsymbol{k}) = \omega_0(k) + \boldsymbol{k}\cdot\boldsymbol{U}(k)\ . \tag{2.2}$$

The functions A, ω_0, $\boldsymbol{U}$, γ, and B are determined from fits to the data. At fixed $\boldsymbol{k}$, with $50 < kR < 200$, the solar spectrum is modeled by the sum of two Lorentz functions with independent amplitudes $A(\boldsymbol{k})$ and $A(-\boldsymbol{k})$ and with central frequencies separated by $2\omega_0 \neq 0$. The frequency shift $\boldsymbol{k}\cdot\boldsymbol{U}$ is interpreted to be a Doppler shift produced by a local horizontal flow $\boldsymbol{U} = (U_x, U_y)$ measured in the frame of reference (rotating at $\Omega_{\rm ref}$). The amplitude is anisotropic and can be parametrized as follows:

$$A(\boldsymbol{k}) = A_0(k) + A_1(k)\cos(\psi - \psi_{\max}) + A_2(k)\cos(2\psi - \alpha)\ . \tag{2.3}$$

The A_2–component includes instrumental astigmatism (a purely spatial distortion) which can not easily be separated from a real solar signal. The A_1–component, however, is of solar origin. We define the *power anisotropy* by the ratio $\eta = 2A_1/A_0$ and the *azimuth of maximum power* by the angle $\psi_{\max}$. The background noise, $B(\boldsymbol{k})$, is small and assumed to be independent of frequency but affected by astigmatism. The half width at half maximum of the Lorentz profile, γ, corresponds to a characteristic e-folding lifetime $\tau = 1/\gamma$. It is not clear whether there are significant ψ-dependent variations in the lifetime.

The values of the parameters are measured at fixed $k = \|\boldsymbol{k}\|$ and λ by a two-dimensional fit to the power spectrum in (ψ, ω)-space. Figure 1 and 2 show fits of the 1997 data for $k = 115/R$ (supergranular scale) at two different latitudes. Notice that power is distributed in two bands at frequencies $\omega = \pm\omega_0 + k(U_x\cos\psi + U_y\sin\psi)$, i.e. two parallel sinusoids. The presumption by Rast *et al.* (2004) that power is distributed in frequency along two intersecting sinusoids is simply inconsistent with the observations.

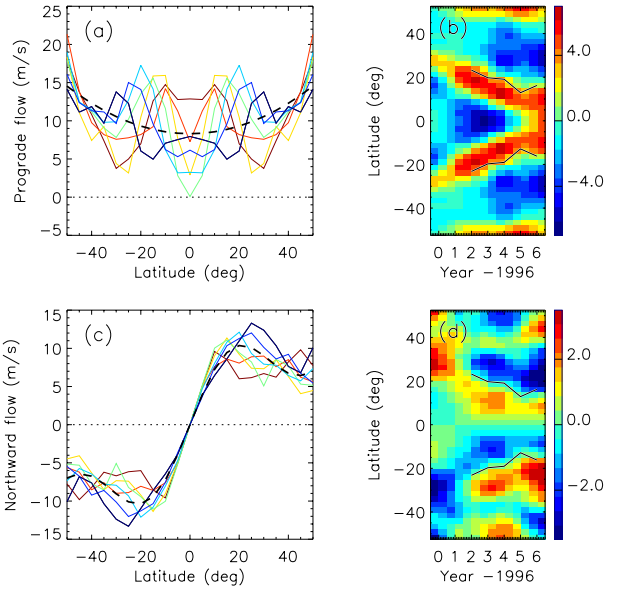

Figure 3. (a) Flow U_x versus λ at $k = 115/R$. Each curve corresponds to a different year (from blue in 1996 to red in 2002). U_x is measured with respect to the reference $R\Omega_{\rm ref}\cos\lambda$. Only the north-south symmetric component is shown. (b) Residuals of U_x after subtraction of a smooth fit (dashed line in panel a). The scale bar has units of $\mathrm{m\,s^{-1}}$. The black curve is an estimate of the mean latitude of activity. (c) Flow U_y versus λ at $k = 115/R$. Only the north-south antisymmetric component is shown. (d) Residual meridional circulation with respect to the dashed line in panel (c). The scale bar has units of $\mathrm{m\,s^{-1}}$.

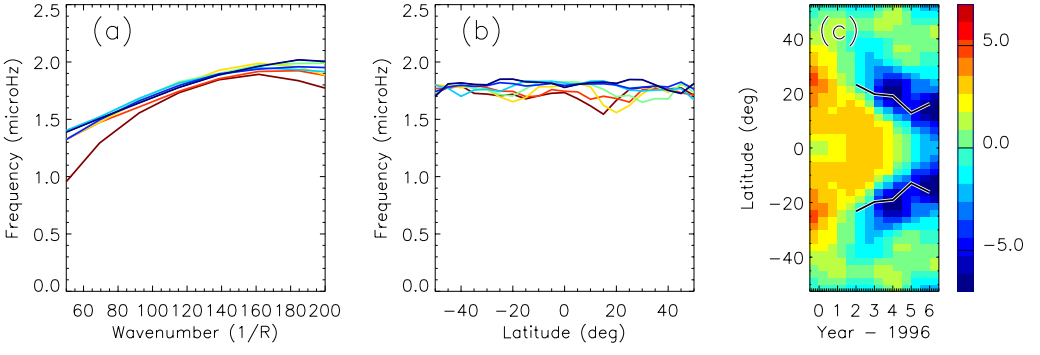

Figure 4. (a) Frequency $\omega_0/2\pi$ versus kR, i.e. dispersion relation. Each curve corresponds to a different year (from blue in 1996 to red in 2002). (b) Frequency $\omega_0/2\pi$ versus λ at $k = 115/R$. (c) Relative change of ω_0, in percent. Only the north-south symmetric component is shown.

3. Results

Figures 3 to 6 show the variations of the background flow, oscillation frequency, lifetime, and anisotropic distribution of power as a function of latitude and time. The measurements confirm and extend the original findings of Gizon *et al.* (2003) and Schou (2003). The dispersion relation, $\omega_0(k)$, varies little with the latitude or the phase of the solar cycle (5% change, Fig. 4c). The lifetime decreases by about 20% at active latitudes (Fig. 5c). Power anisotropy, η, shows a 10% decrease near active regions. Away from the equator,

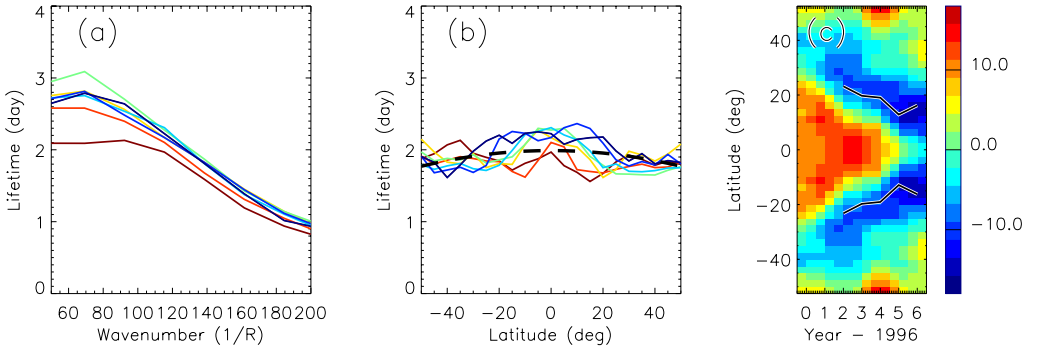

Figure 5. (a) Lifetime, $\tau = 1/\gamma$, versus kR. Each curve corresponds to a different year (from blue in 1996 to red in 2002). (b) Lifetime versus λ at $k = 115/R$. (c) Relative change of τ with respect to the dashed line in panel (b), in percent. Only the north-south symmetric component is shown.

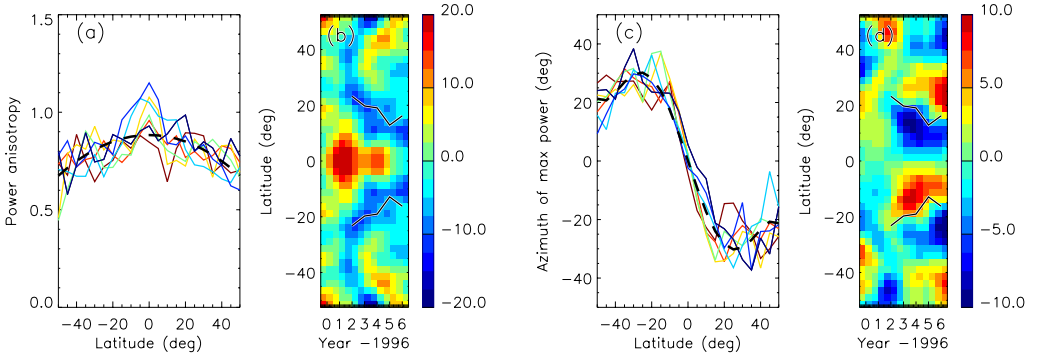

Figure 6. (a) Power anisotropy, $\eta = 2A_1/A_0$, versus λ at $k = 115/R$. Each curve corresponds to a different year (from blue in 1996 to red in 2002). (b) Relative change of η with respect to the dashed line in panel (a), in percent. (c) Azimuth of maximum power, $\psi_{\max}$, versus λ at $k = 115/R$. (d) Residual $\psi_{\max}$ after subtraction of the dashed line in panel (c). The scale bar has units of degrees.

power is maximum in a direction equatorward of the prograde direction (Fig. 6c) and even more so below the mean latitude of activity (Fig. 6d). The large-scale flows, $\boldsymbol{U}$, as defined above, are plotted in Fig. 3. Both zonal and meridional flows are consistent with previous measurements derived from the motion of small magnetic features. The meridional circulation, U_y, is poleward in the supergranular layer and includes a time-varying component converging toward active regions (Fig. 3d). Finally, we repeat that old estimates of rotation and meridional circulation through correlation tracking of the pattern of supergranulation at large time lags are incorrect because they ignore the evolution (propagation) of the pattern (see Gizon & Duvall, 2003). *All figures are in color in the electronic version of the paper.*

References

Duvall, T. L. & Gizon, L. 2000 *Solar Phys.* **192**, 177–191.
Gizon, L. & Duvall, T. L. 2003 in *ESA SP-517*, 43–52
Gizon, L., Duvall, T. L. & Schou, J. 2003 *Nature* **421**, 43–44 (erratum p. 764).
Rast, M. P., Lisle, J. P. & Toomre, J. 2004 *Astrophys. J.* **608**, 1156–1166.
Schou, J. 2003 *Astrophys. J.* **596**, L259–L262.